Volume 14 | Number 30 | 14 August 2016 | Pages 7121–7370

Organic & Biomolecular Chemistry

www.rsc.org/obc

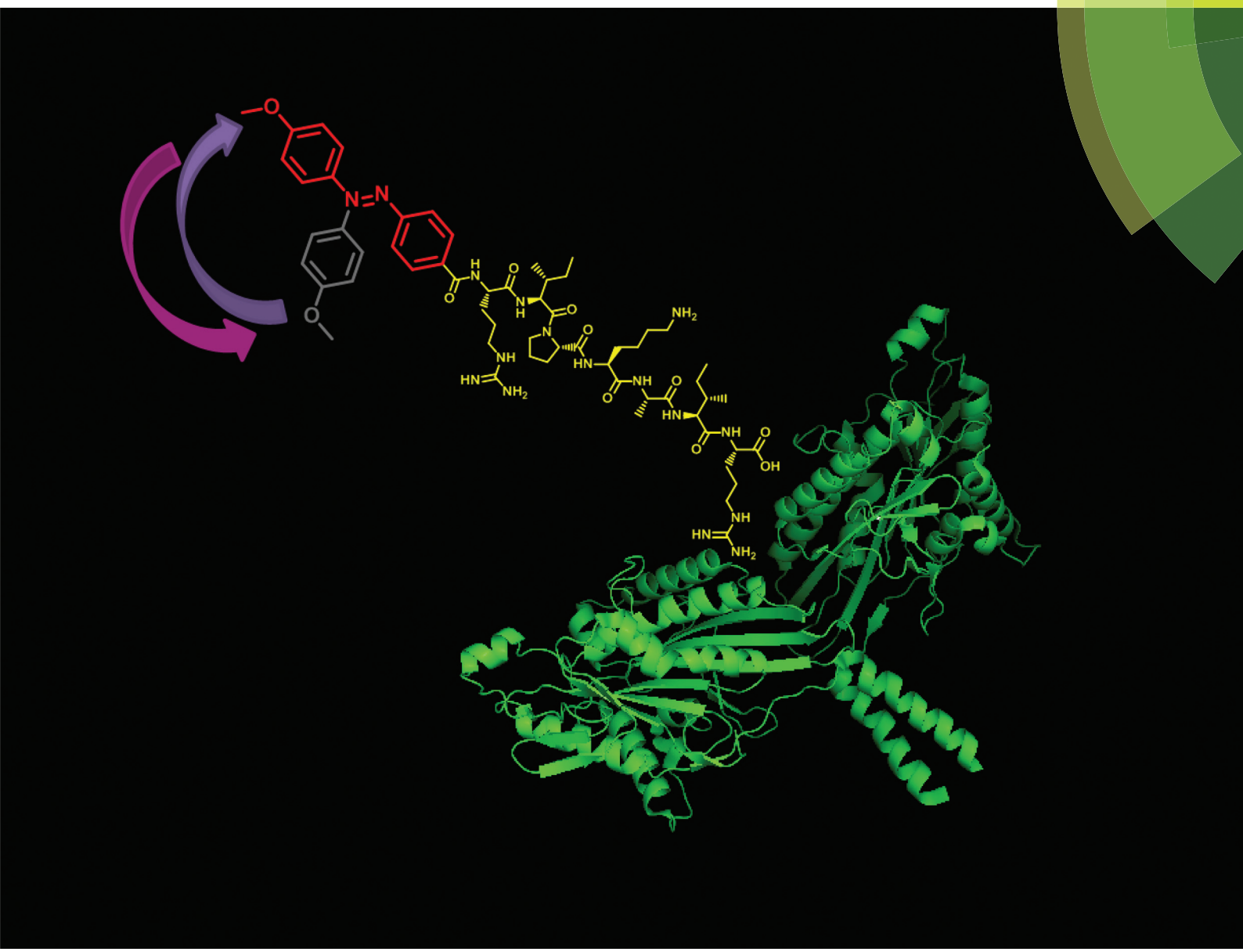

ISSN 1477-0520

ROYAL SOCIETY OF CHEMISTRY

PAPER
Nobuyuki Tamaoki *et al.*
Structure–property relationships of photoresponsive inhibitors of the kinesin motor

175 YEARS

Organic & Biomolecular Chemistry

PAPER

View Article Online
View Journal | View Issue

Open Access Article. Published on 31 May 2016. Downloaded on 8/14/2024 5:04:01 PM.
This article is licensed under a Creative Commons Attribution 3.0 Unported Licence.

Cite this: *Org. Biomol. Chem.*, 2016, **14**, 7202

Structure–property relationships of photoresponsive inhibitors of the kinesin motor†

Ammathnadu S. Amrutha, K. R. Sunil Kumar, Kazuya Matsuo and Nobuyuki Tamaoki*

Received 2nd May 2016,
Accepted 27th May 2016

DOI: 10.1039/c6ob00951d

www.rsc.org/obc

Recently we demonstrated the photoregulation of the activity of kinesin-1 using an azobenzene-tethered peptide (azo-peptide: Azo-Ile-Pro-Lys-Ala-Ile-Gln-Ala-Ser-His-Gly-Arg-OH). To understand the mechanism behind this photoswitchable inhibition, here we studied the structure–property relationships of a range of azo-peptides through systematic variations in the structures of the peptide and azobenzene units. The vital peptide sequence for kinesin inhibition—mediated through electrostatic, hydrophobic and C–H···π interactions—was the same as that for the self-inhibition of kinesin. We also identified substituents on the azobenzene capable of enhancing the photoswitchability of inhibition. As a result, we developed a new inhibitor featuring a relatively short peptide unit (-Arg-Ile-Pro-Lys-Ala-Ile-Arg-OH) and an azobenzene unit bearing a *para*-OMe group. In the *trans* form of its azobenzene unit, this finely tuned inhibitor stopped the kinesin-driven gliding motility of microtubules completely at a relatively low concentration, yet allowed gliding motility with a relatively high velocity in the *cis* form obtained after UV irradiation.

Introduction

Kinesin is an ATP-fuelled biomolecular motor that transports intracellular cargoes (*e.g.*, chromosomes, vesicles, organelles) to specific sites by walking processively along microtubule tracks in living cells.[1–4] Although it has dimensions of only approximately 80 nm, kinesin exhibits excellent force-generating capabilities and converts the chemical energy of ATP into mechanical work with high efficiency.[5–8] Accordingly, the kinesin–microtubule system has found application in artificial nano-transportation systems as molecular shuttles, where the kinesin motors and microtubule filaments have been suitably functionalized for the transport of various nano cargoes.[9–11] Such molecular transport systems can be employed in, for example, sorting, separation, and purification.[6] To enhance the applicability of kinesin as a molecular machine, more complete and precise control over its motor activity will be necessary. Several attempts have already been made in this regard; for example, using a thermo-responsive polymer,[12] electrically switchable polymer surface,[13] caged ATP,[14,15] phototunable non-nucleoside triphosphate energy molecule,[16] caged inhibitory peptides,[17] and enzyme-coated particles that can generate ATP *in situ*.[18] Nevertheless, each of these approaches has suffered from drawbacks related to either one-way regulation or incomplete reversible regulation. Greene *et al.* reported the complete inhibition of mutated kinesin in the presence of Zn^{2+} ions and subsequent reactivation using a metal chelator. The percentage reactivation decreased significantly, however, after the second cycle as a result of the deactivation of kinesin, through either protein denaturation or irreversible inhibition by the Zn^{2+} ions.[19] Complete and reversible regulation over many cycles without any dysfunction would be most desirable.

In living cells, when kinesin is not attached to any cargo, the tail domain bends and binds to the motor domains to avoid the unnecessary consumption of ATP.[17,20–22] Inspired by this self-inhibition mechanism, we derived an inhibitory peptide sequence from the tail domain of kinesin-1 and tethered it to a photoresponsive azobenzene unit at the N-terminus to allow reversible and spatiotemporal regulation of the inhibitory activity through the effects of light irradiation.[23] The large conformational change associated with the photoisomerization of the azobenzene moiety[24–26] led to hugely different affinities for its two different isomeric forms and allowed us to switch the motility on and off completely and reversibly. Nevertheless, we have not previously been in a position to explain precisely the modes of interaction involved in the inhibition by the reverse-ordered peptide; in addition, we had not identified the critical peptide sequence required for inhibition, nor had we examined the effects of substituent groups present on the azobenzene moiety on the inhibitory activity and photoswitchability. For practical applications, we would require more efficient inhibitors that function at lower concentrations with greater photoswitchability. Recently, Kaan *et al.* reported

Research Institute for Electronic Science, Hokkaido University, N20, W10, Kita-Ku, Sapporo, Hokkaido, 001-0020, Japan. E-mail: tamaoki@es.hokudai.ac.jp

†Electronic supplementary information (ESI) available. See DOI: 10.1039/c6ob00951d

This journal is © The Royal Society of Chemistry 2016

Open Access Article. Published on 31 May 2016. Downloaded on 8/14/2024 5:04:01 PM.
This article is licensed under a Creative Commons Attribution 3.0 Unported Licence.

the X-ray crystal structure of the motor domain dimer of *Drosophila melanogaster* kinesin-1 (homologue of human kinesin-1) with the tail peptide.[27] They identified the important amino acid residues and their detailed interactions (electrostatic, hydrophobic, C–H···π) during the self-inhibition mechanism. Interestingly, our earlier-reported inhibitory azo-peptide having the sequence – Azo-Ile-Pro-Lys-Ala-Ile-Gln-Ala-Ser-His-Gly-Arg-OH comprised the important amino acids of the tail peptide of *D. melanogaster* kinesin-1, but in the reverse order. This finding prompted us to examine the behavior of related azo-peptides systematically.

In this study, we determined the important amino acid residues responsible for the inhibition, identified through systematic variations in the structure of the peptide unit, and also investigated the interactions of each of these amino acids that were necessary to induce inhibition. The plausible mechanism of inhibition suggests that the interactions between our azo-peptides and the motor domain are similar to those between the tail domain and the motor domain in the self-inhibition mechanism of kinesin. Among the various substituents appended to the azobenzene unit, we found that the OMe group enhanced the switching properties. Combining these results, we rationally designed a new azo-peptide comprising a shorter peptide sequence (-Arg-Ile-Pro-Lys-Ala-Ile-Arg-OH) coupled to an azobenzene unit substituted with an OMe group at the *para* position. This novel inhibitor stopped the kinesin-driven gliding motility of microtubules completely at a lower concentration (750 μM) in the *trans* form and provided a higher recovery of velocity (86%) in the motility in its *cis* form after UV irradiation.

Results and discussion

Synthesis of azo-peptides

The general procedure for the synthesis of azo-peptides involved solid phase peptide synthesis using the Fmoc strategy.[23] We formed the peptide chains first and then introduced the azobenzene carboxylic acid derivatives at the N-termini through amide linkages. Fig. 1a and b present the reversible isomerization of the azo-peptide and the list of synthesized azo-peptides, respectively. The previously reported azo-peptide **1**[23] was our lead molecule. The azo-peptides **2–6** were designed by removing the N-terminal amino acids one by one to confirm the importance of the -Ile-Pro-Lys-Ala-Ile unit in the inhibition mechanism. We synthesized the azo-peptides **7–11** to clarify the role of the -Ala-Ser-His-Gly-Arg unit: removing the C-terminal amino acids from azo-peptide **1** gave the

(a)

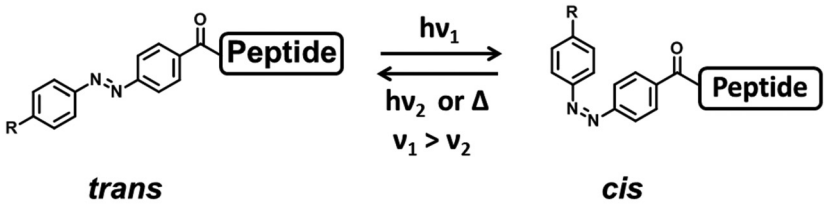

(b)

No.	R[a]	Peptide = $A_1A_2A_3$.....$A_{n-1}A_n$-OH											
1	-H		Ile	Pro	Lys	Ala	Ile	Gln	Ala	Ser	His	Gly	Arg
2	-H			Pro	Lys	Ala	Ile	Gln	Ala	Ser	His	Gly	Arg
3	-H				Lys	Ala	Ile	Gln	Ala	Ser	His	Gly	Arg
4	-H					Ala	Ile	Gln	Ala	Ser	His	Gly	Arg
5	-H						Ile	Gln	Ala	Ser	His	Gly	Arg
6	-H							Gln	Ala	Ser	His	Gly	Arg
7	-H		Ile	Pro	Lys	Ala	Ile	Gln	Ala	Ser	His	Gly	
8	-H		Ile	Pro	Lys	Ala	Ile	Gln					
9	-H		Ile	Pro	Lys	Ala	Ile	Gly					
10	-H		Ile	Pro	Lys	Ala	Ile	Lys					
11	-H		Ile	Pro	Lys	Ala	Ile	Arg					
12	-H	Arg	Ile	Pro	Lys	Ala	Ile	Gln					
13	-H	Arg	Ile	Pro	Lys	Ala	Ile	Arg					
14	-OMe		Ile	Pro	Lys	Ala	Ile	Arg					
15	$-NMe_2$		Ile	Pro	Lys	Ala	Ile	Arg					
16	-COOH		Ile	Pro	Lys	Ala	Ile	Arg					
17	-OMe	Arg	Ile	Pro	Lys	Ala	Ile	Arg					

[a] – Substituent at the *para* position of the azobenzene unit

Fig. 1 (a) Reversible isomerization of azo-peptides. (b) List of synthesized azo-peptides.

Open Access Article. Published on 31 May 2016. Downloaded on 8/14/2024 5:04:01 PM.
This article is licensed under a Creative Commons Attribution 3.0 Unported Licence.

azo-peptides **7** and **8** and replacing the Gln residue in the azo-peptide **8** with Gly, Lys, and Arg residues gave the azo-peptides **9–11**. The azo-peptide **12** was obtained after adding an Arg residue at the N-terminus in the azo-peptide **8**—the crystal structure indicated that an Arg residue interacted more strongly with kinesin motor domains than did a Gln residue, as shown later. The azo-peptide **13** was designed, with reference to the symmetrical recognition of the tail peptide by motor domains, by adding an Arg residue at the C-terminus of the peptide unit of the azo-peptide **12**. The azo-peptides **14–17** featured different substituents at the *para* position of the azobenzene unit. Mass spectra (Fig. S1–S16†) and HPLC chromatograms (Fig. S17†) revealing the purity of the azo-peptides are presented in the ESI.†

Photoisomerization of the azo-peptides and thermal stability of the *cis* isomer

Fig. S18† displays the change in the absorption spectra of the azo-peptides **11** and **14–16** upon photoirradiation. The azo-peptides **11**, **14**, and **16** were reversibly isomerized from their *trans* to *cis* forms and *vice versa* through alternating irradiation with UV and visible lights, respectively, for at least 10 cycles of irradiation without fatigue, as evidenced by consistent UV-Vis spectral profiles. When we irradiated the azo-peptide **15** with visible light to achieve *trans* to *cis* isomerization, we could not detect the *cis*-rich state in its UV-Vis spectrum because the thermal relaxation of the *cis* isomer was faster than the acquisition speed of the spectrophotometer. We examined the thermal stabilities of the *cis* isomers of **14** and **16** by analyzing their absorption spectra at 25 °C in the dark (Fig. S19†). After 1 h, only around 1% of the *trans* forms had been recovered through thermal relaxation of the *cis* isomers, suggesting that thermal relaxation of the *cis* isomers would be negligible over the duration of a motility assay, which is usually complete within 1 h. We used HPLC to measure the conversion ratios for the *trans* to *cis* and *cis* to *trans* transformations upon irradiation with light (Fig. S20† displays the chromatograms). Table 1 lists the isomer ratios in the UV and visible photostationary states (PSSs) of azo-peptides having unsubstituted and OMe- and COOH-substituted azobenzene chromophores (**11**, **14**, and **16**, respectively).

Structure–property relationship

Fig. 2 displays the gliding velocities of the microtubules measured by the gliding motility assay in the *trans* and *cis*-rich states of the azo-peptides at various concentrations in the presence of 1 mM ATP. In the *trans* state of the azo-peptide **1**, the gliding velocity decreased sharply at a concentration of 1.5 mM. At a concentration of 2.5 mM, there was no motility in the pre-irradiated state; in the *cis*-rich state obtained after irradiation with UV light, the microtubules moved with a velocity that was 64% of that in the control experiment (*i.e.*, the velocity measured in the absence of the inhibitor). At this concentration, after irradiation with visible light, the gliding velocity decreased again, but did not reach zero because the concentration of the *trans* isomer in the visible PSS was insufficient to induce complete inhibition [only *ca.* 80% of the *trans* form was obtained in the visible PSS (Table 1)]. When we further increased the concentration of **1** to 3 mM, no motility was evident in either the pre-irradiated state or in the visible PSS. Thus, at a concentration of 3 mM, the motility could be switched completely and reversibly between the ON and OFF states with a 62% recovery of velocity in the motility ON state (Fig. 2a). We calculated the IC_{50} values for ready comparison of the affinities of the *trans* and *cis* isomers for kinesin. For the *trans* isomer of **1**, the IC_{50} was 1.2 mM; for the *cis* isomer, it exceeded 3.5 mM. The azo-peptides **2**, **4–7**, and **9** were insoluble in the buffer; thus, we did not test them in motility assays. Table 2 summarizes the behavior of the synthesized azo-peptides in the *in vitro* motility assays.

Table 1 Isomer ratios in UV and visible PSSs

	UV PSS[a]		Vis PSS[b,c]	
Azo-peptide	*cis*	*trans*	*cis*	*trans*
11	87.4%	12.6%	20.8%	79.2%
14	95.5%	4.5%	29.7%	70.3%
16	73.1%	26.9%	9.0%	91.0%

[a] 365 nm. [b] 436 nm for **11** and **16**. [c] 510 nm for **14**.

Repeatability of gliding motility photoregulation

The azo-peptide **17** induced complete inhibition at a submillimolar concentration (750 μM) with 86% recovery of the gliding velocity in the motility ON state. With this azo-peptide, we performed an experiment including four cycles of alternating irradiation with UV and visible light for 5 and 10 s, respectively. Fig. 3 displays the gliding velocities of the microtubules calculated after each irradiation with UV and visible light. Prior to irradiation, all of the microtubules were in the OFF state. After irradiation with UV light, they were moving with an average velocity of 0.43 μm s^{-1}. After subsequent irradiation with visible light, the gliding velocity of the microtubules again reached zero. No significant decrease in the recovery velocity in the motility ON state was evident after the fourth irradiation cycle. The motility can be switched ON and OFF completely for at least 10 cycles in the *in situ* photoregulation experiment shown below (the data is not included here).

In situ photoregulation of gliding motility

Using the azo-peptide **17** at a concentration of 750 μM in BRB-80 buffer in the presence of 1 mM ATP, we performed a gliding motility experiment in which we recorded a video for 6 min (Movie in the ESI†) while performing multiple cycles of irradiation with UV and visible light. The ON and OFF switching of motility was achieved through alternating irradiation at 365 nm for 1 s and at 510 nm for 3 s, respectively. Prior to irradiation with UV light, we observed a complete OFF state for the microtubules. After 1 min, when the flow cell had been irradiated with light at 365 nm for 1 s, all of the microtubules

 This journal is © The Royal Society of Chemistry 2016

Open Access Article. Published on 31 May 2016. Downloaded on 8/14/2024 5:04:01 PM.
This article is licensed under a Creative Commons Attribution 3.0 Unported Licence.

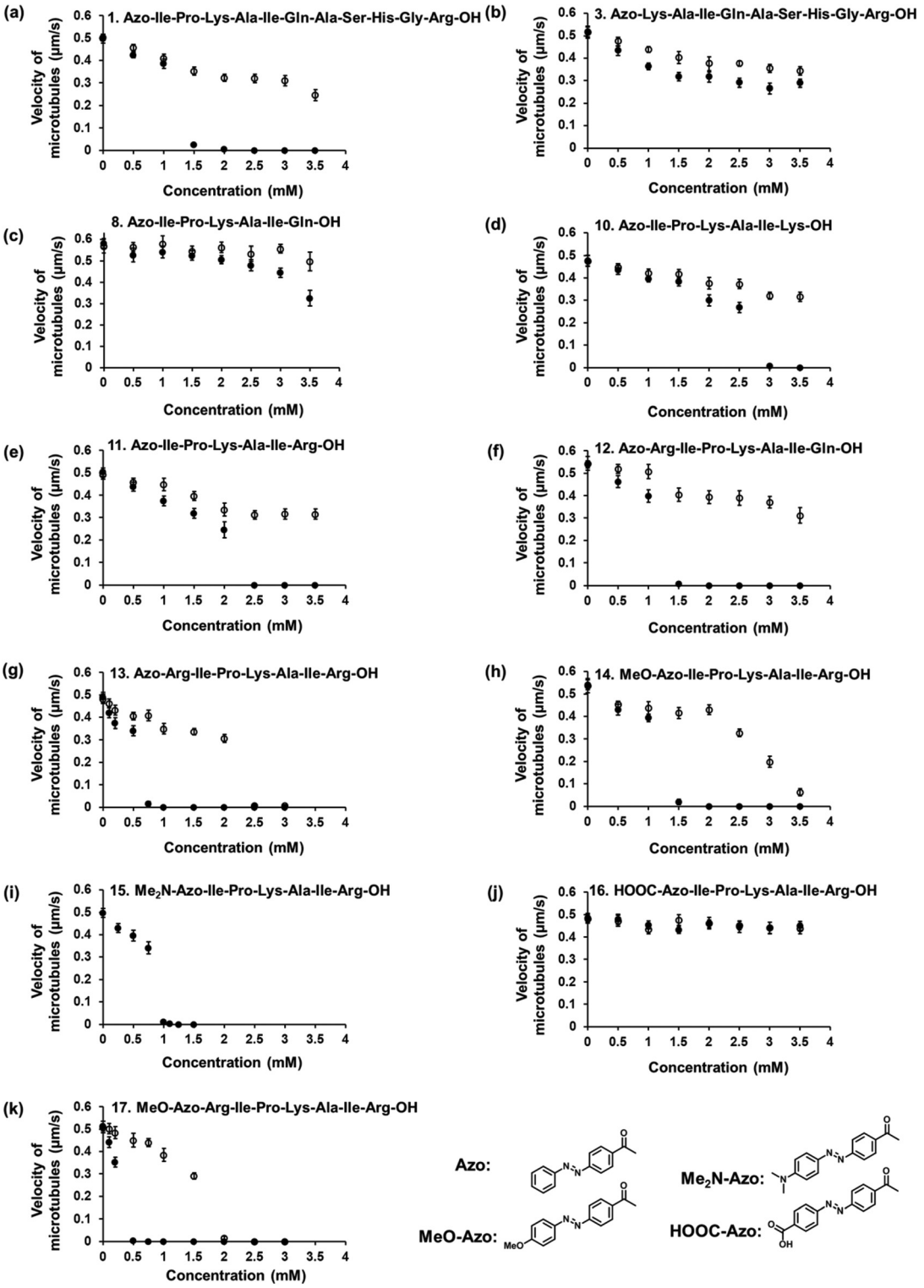

Fig. 2 Gliding velocities of microtubules plotted with respect to the concentrations of the azo-peptides (solid circles: velocity of microtubules in the *trans* state; open circles: velocity in the *cis*-rich state). Error bars represent the standard deviations for 10 microtubules in a single flow cell.

were in motion, with the elimination of their gliding motion after irradiation for 3 s with light at 510 nm. Fig. 4 highlights the motion of two selected microtubules that did not change positions for 60 s prior to irradiation, but did change their positions after irradiation with UV light and then, again, remained motionless after irradiation with visible light.

For self-inhibition, the tail domain interacts with the kinesin motor domains through noncovalent interactions.

Open Access Article. Published on 31 May 2016. Downloaded on 8/14/2024 5:04:01 PM.
This article is licensed under a Creative Commons Attribution 3.0 Unported Licence.

Table 2 Solubility and inhibitory behavior of azo-peptides

Azo-peptide	Solubility at 22.0 mM[a]	IC_{50} (mM) *trans*	IC_{50} (mM) *cis*	Minimum concentration displaying ON/OFF switching of motility (mM)	Recovery of velocity in the motility ON state[b] (%)
1	S	1.2	>3.5	3.0	62 ± 5
2	I	—	—	—	—
3	G	>3.5	>3.5	>3.5	—
4	I	—	—	—	—
5	I	—	—	—	—
6	I	—	—	—	—
7	I	—	—	—	—
8	S	>3.5	>3.5	>3.5	—
9	I	—	—	—	—
10	S	2.6	>3.5	3.5	66 ± 4
11	S	2.1	>3.5	3.0	62 ± 5
12	S	1.1	>3.5	2.5	72 ± 6
13	S	0.6	2.1	1.5	70 ± 3
14	S	1.2	3.0	2.0	80 ± 4
15	S	0.8	—	1.25	0[c]
16	S	>3.5	>3.5	>3.5	—
17	S	0.2	1.6	0.75	86 ± 3

[a] In BRB-80 buffer at room temperature: S, soluble; I, insoluble; G, initially soluble but after some time forms a gel. [b] Recovery velocity measured at the minimum inhibitor concentration displaying the ON/OFF switching of motility. [c] No velocity recovery observed because of the rapid thermal relaxation of the *cis* isomer (*i.e.*, motility not observed).

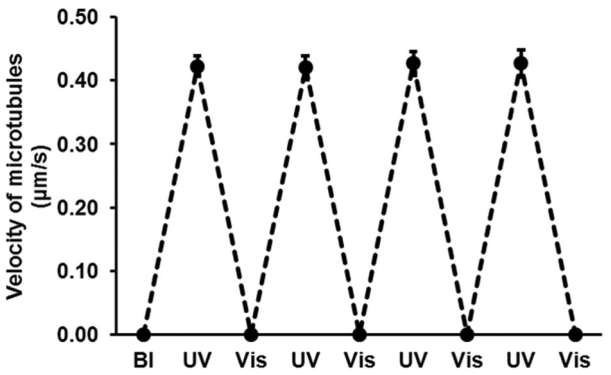

Fig. 3 Repeatability of the complete and reversible photoregulation of the microtubule gliding velocity for the azo-peptide **17** (750 μM) in the presence of 1 mM ATP (BI: before irradiation; UV: after irradiation with 365 nm light; Vis: after irradiation with 510 nm light). Error bars: standard deviation for 10 microtubules.

X-ray crystallography of *D. melanogaster* kinesin-1 with the tail peptide (-^{940}Ala-Gln-Ile-Ala-Lys-Pro-Ile-Arg^{948}Ser-) revealed that the tail peptide is almost symmetrical with respect to ^{944}Lys of the tripeptide Ile-Ala-Lys core. This Ile-Ala-Lys core is highly conserved in kinesin-1s and regarded as both a necessary and sufficient condition for inducing inhibition.[20,21,28,29] The center residue ^{944}Lys in the tail peptide interacts electrostatically with residue ^{185}Asp of the motor domain. The two isoleucine residues in the tail peptide interact with the two hydrophobic pockets composed of residues ^{123}Phe, ^{126}Ile, and ^{135}Phe of both motor domains. A C–H···π interaction exists between residue ^{945}Pro of the tail and residue ^{179}Phe of the motor domain (Fig. 5b and c). Human kinesin-1 is highly conserved with *D. melanogaster* kinesin-1 (Fig. S21†). The critical interaction sites mentioned above are well preserved, although only residue ^{185}Asp in *D. melanogaster* kinesin-1 is replaced by ^{178}Glu in human kinesin-1. Because of the high similarity, we can apply almost the same mechanism to the tail-mediated inhibition of human kinesin-1. Interestingly, in the crystal structure, the tail peptide occupied the interface composed of the symmetrical dimer of motor domains[30–32] in two different modes. One is N→C (N terminus to C terminus), while the other is the opposite sequence: that is, the C←N peptide. The overlay of the N→C and C←N tail peptides in Fig. 5(a) reveals little difference in their structures. Both of the peptides are acceptable by the motor domain dimer, indicating that the main chain of the tail peptide does not have a great influence on the binding of the tail peptide. The previously reported azo-peptide **1** (Azo-Ile-Pro-Lys-Ala-Ile-Gln-Ala-Ser-His-Gly-Arg-OH) has the reverse sequence of the natural tail domain (-^{914}Arg-Gly-His-Ser-Ala-Gln-Ile-Ala-Lys-Pro^{925}Ile-). Thus, inhibition by the azo-peptide **1** presumably occurred through the same mechanism as that of the natural tail peptide. The azo-peptide **1** contains all of the important amino acid residues in the sequence -Ile-Pro-Lys-Ala-Ile-Gln-, with the photoresponsive azobenzene moiety placed sufficiently closely nearby to facilitate a huge difference in affinity between the two isomeric forms of the azo-peptide.

A comparison of the inhibitory behavior of the azo-peptides **1** and **3** suggests that the amino acid residues Ile and Pro adjacent to the highly conserved Lys-Ala-Ile core (-**Ile-Pro-Lys-Ala-Ile**-Gln-) are important to achieve inhibition, because the inhibition property decreased significantly by removing these residues from the sequence (Fig. 2a and b). The insolubility of the azo-peptide **7** and the inefficiency of the azo-peptide **8** at inducing inhibition suggested the need to modify the natural sequence. The azo-peptide **9**, with a Gly residue at the C-terminus, rather than a Gln residue, was insoluble, whereas the azo-peptides **10** and **11**, featuring basic amino acid residues (Lys and Arg, respectively) at the C-terminus, rather than the Gln residue, provided complete inhibition at concentrations of 3.5 and 3.0 mM, respectively (Fig. 2d and e). These observations suggest that the key residue in human kinesin motor domains is the acidic ^{170}Glu residue, as displayed in Fig. 5d and S21b.† Because the Arg residue is relatively basic, its interaction with residue ^{170}Glu was stronger than that of a Lys residue. Enhanced inhibition occurred with the azo-peptide **12**, which displayed complete inhibition at a relatively low concentration (2.5 mM, Fig. 2f) compared with that of the azo-peptide **8**, which lacks the Arg residue at the N-terminus (Fig. 2c); thus, to improve affinity, an additional Arg residue at the N-terminus was quite effective. As a result, the azo-peptide **13**, for which the peptide unit -Arg-Ile-Pro-Lys-Ala-Ile-Arg is symmetrical with respect to the central Lys residue, exhibited inhibition behavior stronger than that of the azo-peptide **12**, completely inhibiting the kinesin motor at a concentration of 1.5 mM (Fig. 2g

 This journal is © The Royal Society of Chemistry 2016

Open Access Article. Published on 31 May 2016. Downloaded on 8/14/2024 5:04:01 PM.
This article is licensed under a Creative Commons Attribution 3.0 Unported Licence.

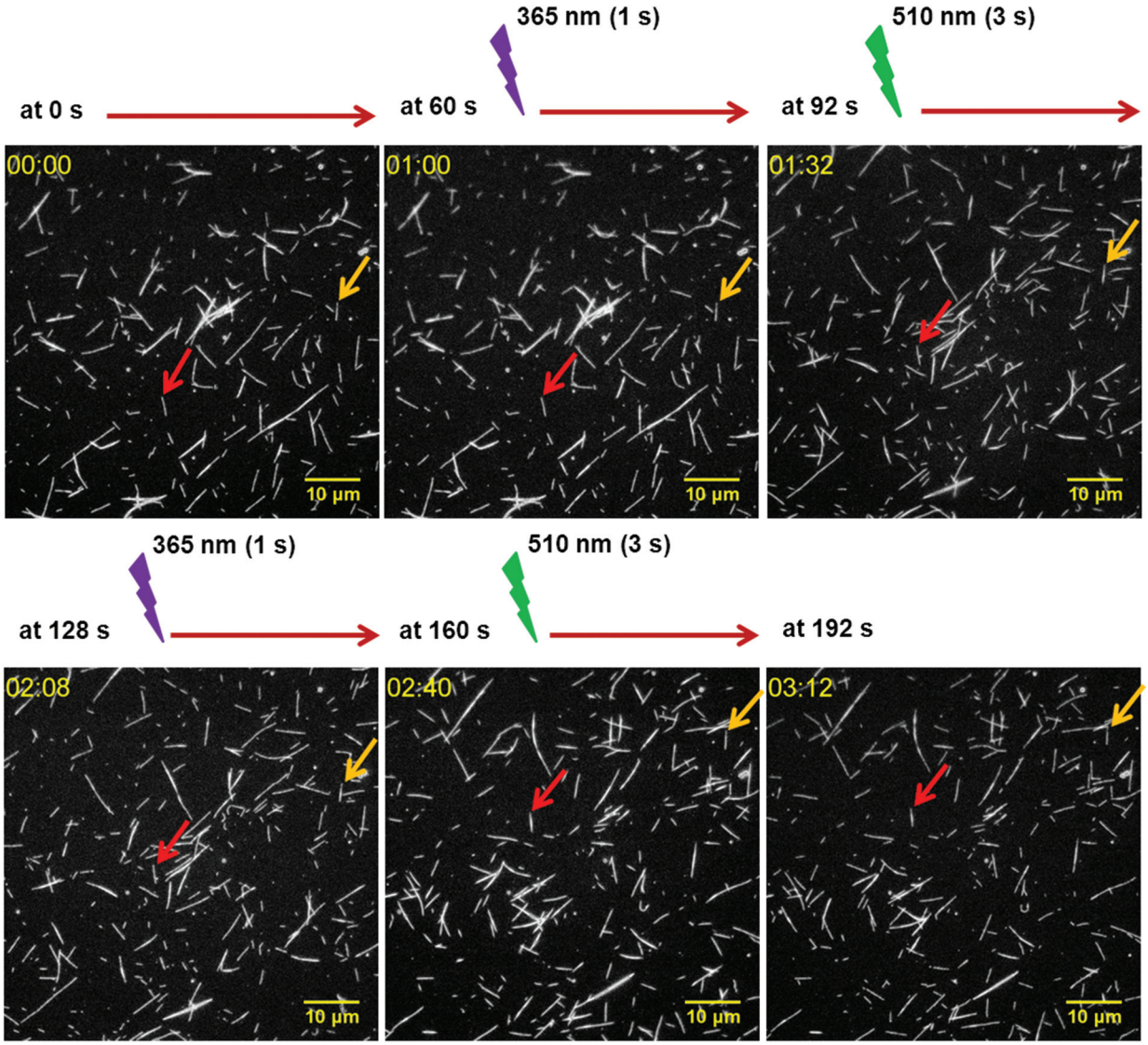

Fig. 4 Fluorescence images displaying the ON and OFF states of the gliding motility of microtubules in the *in situ* photoregulation experiment using the azo-peptide **17** (750 μM) in the presence of 1 mM ATP and alternating irradiation at 365 nm (for 1 s) and 510 nm (for 3 s). Red and yellow arrows highlight the positions of two selected microtubules.

and f). Fig. 5d displays a plausible mode of interaction experienced by the azo-peptide **13**.

The inhibition properties were enhanced, relative to those of the parent azo-peptide **11**, after substitution with OMe and NMe_2 groups: the azo-peptides **14** and **15** induced complete inhibition at concentrations of 2 and 1.25 mM, respectively (Fig. 2h and i). This behavior represents the relatively greater affinities of these two azo-peptides towards the kinesin. By substituting with an OMe or NMe_2 group, we added an additional moiety that could function as a proton acceptor for hydrogen bonding with the kinesin pocket. The recovery of velocity of the azo-peptide **14**, with the OMe substituent, was higher (*ca*. 80%) in the motility ON state than that of the azo-peptide **11** (recovery of velocity: 62%). This behavior was due to the higher percentage of the *cis* form (95.5%) in the UV PSS for the compound having the OMe group at the *para* position of the azobenzene unit than that for the unsubstituted-azobenzene azo-peptide (87.4% *cis* form in the UV PSS; Table 1). In the case of the azo-peptide **15**, bearing an NMe_2 group, we could not switch the system into the motility ON state because of the rapid thermal relaxation of the *cis* isomer and the insufficient intensity of the irradiated light.[33] The azo-peptide **16**, substituted with a COOH group, did not display any inhibition effect, even though it featured the amino acid sequence responsible for the inhibitory activity (Fig. 2j), indicating that the interaction site in kinesin does not favor negatively charged substituents on the azobenzene unit.

Finally, from our study of the structure–property relationships, we rationally designed the azo-peptide **17** to feature the peptide unit -Arg-Ile-Pro-Lys-Ala-Ile-Arg-OH and a *para*-OMe

Open Access Article. Published on 31 May 2016. Downloaded on 8/14/2024 5:04:01 PM.
This article is licensed under a Creative Commons Attribution 3.0 Unported Licence.

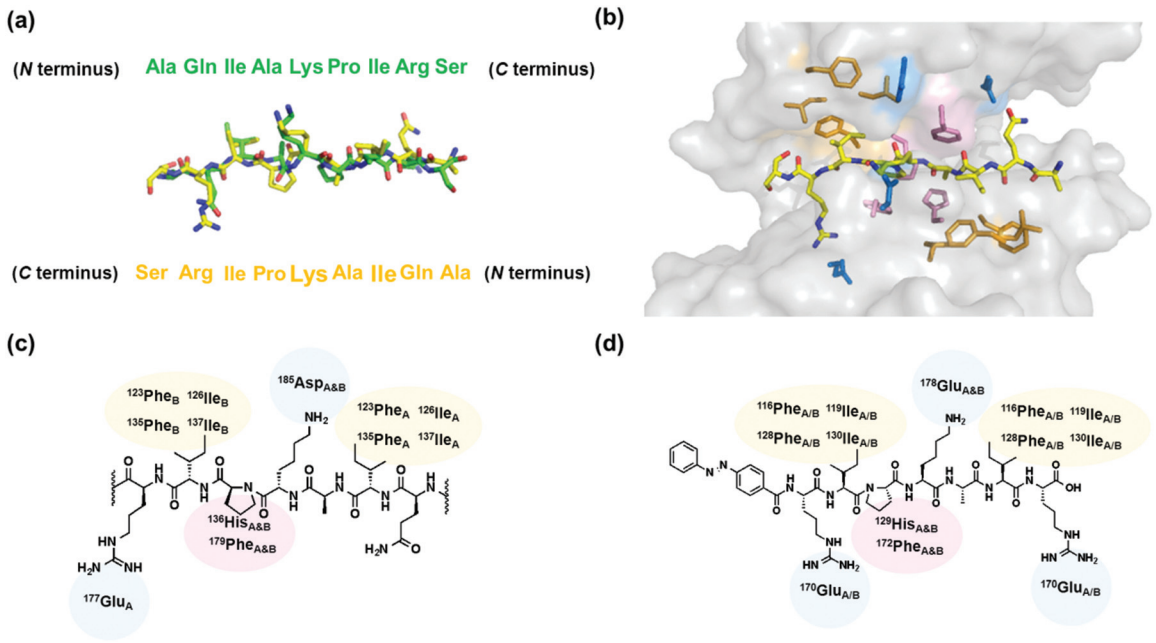

Fig. 5 (a) Overlay of N→C and C←N tail peptides of *D. melanogaster* kinesin-1 (PDB: 2Y65). (b) Interaction of the tail peptide with the *D. melanogaster* kinesin-1 motor domain (in the kinesin motor domain: brown, hydrophobic amino acids; blue, acidic amino acids; pink, aromatic amino acids). (c) Schematic representation of the peptide's interactions with the amino acid residues of the kinesin interface. (d) Plausible interactions between the azo-peptide **13** and the human kinesin motor domains.

group on the azobenzene unit. We anticipated that this structure would fulfill the plausible mechanism of azo-peptide inhibition displayed in Fig. 5d. Indeed, the azo-peptide **17** induced complete inhibition of kinesin at a concentration of 750 μM—in other words, it had four times the affinity of the azo-peptide **1**. In the motility ON state, **17** attained a relatively high recovery of velocity (86%); its percentage recovery remained unchanged even after the fourth cycle of motility switching (Fig. 3). Thus, through *in situ* photoregulation experiments, we have demonstrated the rapid, complete, reversible, and spatiotemporal regulation of the gliding motility of kinesin over several cycles with constant activity (Fig. 4).

Conclusions

Through the systematic design and analysis of the activities of several azo-peptides, we have identified the amino acid residues responsible for the inhibition of kinesin motility and have developed a plausible mechanism for inducing the inhibition. The interactions observed in the mechanism of inhibition induced by the azo-peptides are similar to those in the natural tail-mediated self-inhibition of kinesin. Among the different substituents tested on the azobenzene unit, the OMe group enhanced the inhibition properties and provided a large phototunable change in activity. Taking all of our findings together, we designed a new photoresponsive inhibitor **17** to feature a shorter sequence (-Arg-Ile-Pro-Lys-Ala-Ile-Arg-OH) and an azobenzene moiety substituted with a *para*-OMe group. This azo-peptide stopped the kinesin-propelled gliding motility of microtubules completely in the *trans* form of the azobenzene unit at a concentration of 750 μM, while in the *cis* form of the azobenzene unit it allowed the gliding motility of microtubules with 86% recovery of velocity with respect to the velocity observed in the non-inhibited state of the kinesin.

Experimental

Chemicals

All chemical and biochemical reagents were purchased from commercial sources (Tokyo Chemical Industry; Watanabe Chemical Industries; Wako Pure Chemical Industries; Dojindo Molecular Technologies) and used without purification.

Instrumentation

A Burrell Wrist Action Shaker (model 75) was used for the azo-peptide synthesis. Purification and analysis of the azo-peptides were performed using a Shimadzu reversed-phase (RP) HPLC system. An EYELA FDU-2200 lyophilization system was used for freeze-drying. Electrospray ionization time-of-flight mass spectrometry (ESI-TOF MS) was performed using a JMS-T100CS instrument (JEOL) operated in the positive-ion mode. UV-Vis absorption spectra were recorded using an Agilent 8453 single-beam spectrophotometer and a Hitachi U-3100 absorption spectrophotometer. A mercury lamp (Ushio) with band pass filters for 436 and 365 nm was used for photoisomerization experiments. A Hamamatsu LED Controller (model C11924-101) for 365 nm light and a Hayasaka LED Controller (model CS_LED 3W_510) for 510 nm light were

 This journal is © The Royal Society of Chemistry 2016

Open Access Article. Published on 31 May 2016. Downloaded on 8/14/2024 5:04:01 PM.
This article is licensed under a Creative Commons Attribution 3.0 Unported Licence.

used for the *in situ* photoregulation experiments. An inverted fluorescence optical microscope (Olympus IX71) equipped with a UPlan F1 100×/1.30 oil C1 objective lens (Olympus) was used for the motility experiments in conjunction with appropriate filters (640 nm excitation filter). An EMCCD digital camera (Andor Solis Technology, model DL-604M-0EM-H1) was used to record videos.

Synthesis

Synthesis of azobenzene derivatives. 4-((4-Methoxyphenyl) diazenyl)benzoic acid and azobenzene-4,4′-dicarboxylic acid were synthesized according to previously reported procedures.[34,35]

Synthesis of azo-peptides. The azo-peptides were synthesized through solid phase peptide synthesis (SPPS) using a standard Fmoc-based SPPS protocol, as reported earlier.[23] Fmoc-Ala-OH, Fmoc-Gln(Mbh)-OH, Fmoc-Gly-OH, Fmoc-His(Boc)-OH, Fmoc-Ile-OH, Fmoc-Arg(Pbf)-OH, Fmoc-Lys(Boc)-OH, Fmoc-Pro-OH, and Fmoc-Ser(*t*Bu)-OH were used as building blocks (Pbf: 2,2,4,6,7-pentamethyldihydrobenzofurane-5-sulfonyl; Boc: *tert*-butyloxycarbonyl; Mbh: 4,4′-dimethoxybenzhydryl). Alko-resin preloaded with the first amino acid was treated with 20% piperidine in *N*,*N*-dimethylformamide (DMF, 4 mL) to deprotect the N-terminus Fmoc amino group. Coupling reactions were performed with a mixture of an Fmoc amino acid (4 eq.), *O*-(benzotriazol-1-yl)-*N*,*N*,*N*,*N*-tetramethyluronium hexafluorophosphate (HBTU, 4 eq.), 1-hydroxy-1*H*-benzotriazole monohydrate (HOBt·H_2O, 4 eq.), and *N*,*N*-diisopropylethylamine (DIPEA, 8 eq.) in DMF for 1 h at room temperature. All coupling and deprotection reactions were checked through Kaiser tests. After elongation of the peptide, an azobenzene derivative presenting a carboxylic acid group was introduced at the N-terminus of the peptide. The azo-peptide was cleaved from the resin using reagent-K [trifluoroacetic acid (TFA)/phenol/thioanisole/H_2O/triisopropylsilane, 8.25 : 0.5 : 0.5 : 0.5 : 0.25] and precipitated in cold diethyl ether. The crude azo-peptide was purified using the RP-HPLC system.

Characterization of azo-peptides

The synthesized azo-peptides were analyzed for their purity using the RP-HPLC system (column: $5C_{18}$-MS-II, 4.6 × 250 mm (Nacalai Tesque); eluent: CH_3CN/H_2O with 0.1% TFA; solvent gradient: 20–45% CH_3CN in water, over 1 h; flow rate: 1 mL min^{-1}; injection volume: 20 μL; monitoring wavelengths: 283, 305, 284, and 480 nm (for the azo-peptides bearing azobenzene units with H, OMe, COOH, and NMe_2 substituents, respectively, at their *para* positions)). ESI-TOF mass spectra of the azo-peptides were recorded.

In vitro motility experiments

Gliding motility assays were performed at 25 °C using the standard protocol described previously,[23] but with BRB-80 [pH 6.9; piperazine-1,4-bis(2-ethanesulfonic acid) (PIPES), 80 mM; $MgCl_2$, 2 mM; *O*,*O*-bis(2-aminoethyl)ethyleneglycol-*N*,*N*,*N*′,*N*′-tetraacetic acid (EGTA), 1 mM] as the assay buffer. For the azo-peptides **1–13**, light at wavelengths of 365 and 436 nm (Hg lamp) was irradiated for 20 and 40 s, respectively. For the azo-peptide **16**, light at wavelengths of 365 and 436 nm (Hg lamp) was irradiated for 40 and 20 s, respectively. The intensities of the 365 and 436 nm light (Hg lamp) were approximately 9.1 and 26.5 mW cm^{-2}, respectively. For the azo-peptides **14** and **17**, light at wavelengths of 365 and 510 nm (LED), with intensities of approximately 1 and 0.46 W cm^{-2}, respectively, was irradiated for 7 and 15 s, respectively. A video was recorded after photoirradiating the flow cell to reach the respective PSSs. Videos were analyzed using ImageJ software. The gliding velocity was determined from the average of 10 measurements.

In situ photoregulation of the gliding velocity of microtubules

A flow cell was prepared containing kinesin, microtubules, oxygen scavengers, ATP (1.0 mM), and the azo-peptide **17** (750 μM). Repeated photoswitching was performed through irradiation with UV light (365 nm, LED) for 1 s and with visible light (510 nm, LED) for 3 s. A video was recorded continuously for 6 min.

Acknowledgements

We thank Professor Takashi Kamei (Hokuriku University) for kindly providing human kinesin-1 and tubulin labeled with CF633 succinimidyl ester.

References

1 R. D. Vale, T. S. Reese and M. P. Sheetz, *Cell*, 1985, **42**, 39–50.
2 S. T. Brady, *Nature*, 1985, **317**, 73–75.
3 N. Hirokawa, Y. Noda and Y. Okada, *Curr. Opin. Cell Biol.*, 1998, **10**, 60–73.
4 M. Schliwa and G. Woehlke, *Nature*, 2003, **422**, 759–765.
5 H. Hess, G. D. Bachand and V. Vogel, *Chem. – Eur. J.*, 2004, **10**, 2110–2116.
6 M. G. L. van den Heuvel and C. Dekker, *Science*, 2007, **317**, 333–336.
7 D. J. G. Bakewell and D. V. Nicolau, *Aust. J. Chem.*, 2007, **60**, 314–332.
8 S. Aoyama, M. Shimoike and Y. Hiratsuka, *Proc. Natl. Acad. Sci. U. S. A.*, 2013, **110**, 16408–16413.
9 A. Agarwal and H. Hess, *Prog. Polym. Sci.*, 2010, **35**, 252–277.
10 H. Hess, *Annu. Rev. Biomed. Eng.*, 2011, **13**, 429–450.
11 G. D. Bachand, N. F. Bouxsein, V. Vandelinder and M. Bachand, *Wiley Interdiscip. Rev.: Nanomed. Nanobiotechnol.*, 2014, **6**, 163–177.
12 L. Ionov, M. Stamm and S. Diez, *Nano Lett.*, 2006, **6**, 1982–1987.
13 B. D. Martin, L. M. Velea, C. M. Soto, C. M. Whitaker, B. P. Gaber and B. Ratna, *Nanotechnology*, 2007, **18**, 055103–055109.
14 H. Higuchi, E. Muto, Y. Inoue and T. Yanagida, *Proc. Natl. Acad. Sci. U. S. A.*, 1997, **94**, 4395–4400.

Open Access Article. Published on 31 May 2016. Downloaded on 8/14/2024 5:04:01 PM.
This article is licensed under a Creative Commons Attribution 3.0 Unported Licence.

15 H. Hess, J. Clemmens, D. Qin, J. Howard and V. Vogel, *Nano Lett.*, 2001, **1**, 235–239.
16 N. Perur, M. Yahara, T. Kamei and N. Tamaoki, *Chem. Commun.*, 2013, **49**, 9935–9937.
17 A. Nomura, T. Q. P. Uyeda, N. Yumoto and Y. Tatsu, *Chem. Commun.*, 2006, **1**, 3588–3590.
18 Y.-Z. Du, Y. Hiratsuka, S. Taira, M. Eguchi, T. Q. P. Uyeda, N. Yumoto and M. Kodaka, *Chem. Commun.*, 2005, **2**, 2080–2082.
19 A. C. Greene, A. M. Trent and G. D. Bachand, *Biotechnol. Bioeng.*, 2008, **101**, 478–486.
20 D. L. Coy, W. O. Hancock, M. Wagenbach and J. Howard, *Nat. Cell Biol.*, 1999, **1**, 288–292.
21 D. D. Hackney and M. F. Stock, *Nat. Cell Biol.*, 2000, **2**, 257–260.
22 M. F. Stock, J. Guerrero, B. Cobb, C. T. Eggers, T. Huang, X. Li and D. D. Hackeny, *J. Biol. Chem.*, 1999, **274**, 14617–14623.
23 K. R. S. Kumar, T. Kamei, T. Fukaminato and N. Tamaoki, *ACS Nano*, 2014, **8**, 4157–4165.
24 A. a. Beharry and G. A. Woolley, *Chem. Soc. Rev.*, 2011, **40**, 4422–4437.
25 H. M. D. Bandara and S. C. Burdette, *Chem. Soc. Rev.*, 2012, **41**, 1809–1825.
26 E. Merino and M. Ribagorda, *Beilstein J. Org. Chem.*, 2012, **8**, 1071–1090.
27 H. Y. K. Kaan, D. D. Hackney and F. Kozielski, *Science*, 2011, **333**, 883–885.
28 H. Yonekura, A. Nomura, H. Ozawa, Y. Tatsu, N. Yumoto and T. Q. P. Uyeda, *Biochem. Biophys. Res. Commun.*, 2006, **343**, 420–427.
29 D. D. Hackney, N. Baek and A. C. Snyder, *Biochemistry*, 2009, **48**, 3448–3456.
30 J. T. Yang, R. A. Laymon and L. S. B. Goldstein, *Cell*, 1989, **56**, 879–889.
31 T. G. Huang, J. Suhan and D. D. Hackney, *J. Biol. Chem.*, 1994, **269**, 16502–16507.
32 M. De Cuevas, T. Tao and L. S. B. Goldstein, *J. Cell Biol.*, 1992, **116**, 957–965.
33 Y. J. Lee, S. I. Yang, D. S. Kang and S. W. Joo, *Chem. Phys.*, 2009, **361**, 176–179.
34 S. Prathap Chandran, F. Mondiot, O. Mondain-Monval and J.-C. Loudet, *Langmuir*, 2011, **27**, 15185–15198.
35 M. L. Tomlinson, *J. Chem. Soc.*, 1946, 756.

This journal is © The Royal Society of Chemistry 2016